Ab initio study of magnetic coupling in $CaCu_3B_4O_{12}$ (B = Ti, Ge, Zr, and Sn)

Masayuki Toyoda,[1,2,*] Kunihiko Yamauchi,[2] and Tamio Oguchi[1,2]

[1]*CREST, Japan Science and Technology Agency, 7, Gobancho, Chiyoda-ku, Tokyo 102-0076, Japan*

[2]*The Institute of Scientific and Industrial Research, Osaka University, 8-1, Mihogaoka, Ibaraki, Osaka 567-0047, Japan*

(Received 1 April 2013; revised manuscript received 29 May 2013; published 27 June 2013)

Magnetism of A-site-ordered perovskites, $CaCu_3Ti_4O_{12}$, $CaCu_3Ge_4O_{12}$, $CaCu_3Sn_4O_{12}$, and $CaCu_3Zr_4O_{12}$, is comprehensively studied by means of *ab initio* electronic structure calculations. The magnetic exchange coupling constants between Cu-site spins, J_1, J_2, and J_3, are estimated within an effective Heisenberg model, revealing relative importance of J_3 despite its long interaction length. The ground-state magnetic order is reasonably explained by the combination of (i) relatively weak ferromagnetic superexchange interaction (J_1) that works for all the oxides and (ii) antiferromagnetic long-range superexchange interaction (J_3) that works selectively for $CaCu_3Ti_4O_{12}$ and $CaCu_3Zr_4O_{12}$.

DOI: 10.1103/PhysRevB.87.224430 PACS number(s): 31.15.E−, 75.30.Et, 75.10.Jm

I. INTRODUCTION

Perovskite oxides, which have the general formula ABO_3, exhibit a wide range of functional properties, such as high-temperature superconductivity,[1] colossal magnetoresistivity,[2,3] ferroelectricity,[4] and multiferroicity.[5] Transition-metal cations typically occupy the octahedrally coordinated B site, which is magnetically coupled via superexchange interaction. The physical properties of perovskite oxides can be tuned by chemical substitution as well as carrier doping. For example, double perovskite structure $A_2BB'O_6$ with two different kinds of B-site transition-metal ions allows us to utilize much broader compositional diversity.[6] A-site-ordered perovskites $AA'_3B_4O_{12}$ are another derivative of perovskite (also called as *quadruple perovskite*[7]), generally crystallizing with the space group of $Im\bar{3}$, as shown in Fig. 1. The A and A' sites, both of which are 12-fold-coordinated A sites in the original perovskite structure, make an ordered structure with 1:3 composition. The BO_6 octahedra undergo tilting so that the coordination of O^{2-} ions around A' site becomes fourfold square planar, while that around A site remains as 12-fold coordination. Consequently, the Jahn-Teller ions such as Cu^{2+} and Mn^{3+} can be accommodated in A' sites. The A'- and B-site ions form different magnetic sublattices and the coexistence of the magnetic interactions between A'-A', A'-B, and B-B sublattices is expected to give rise to intriguing magnetic structure. In this paper, we focus on the magnetic interaction within the A'-site sublattice as it has not been extensively discussed in the past, in contrast to the perovskite B-site sublattice that has been comprehensively understood.[8,9]

The $CaCu_3B_4O_{12}$ family with magnetic Cu^{2+} ions at A' site and nonmagnetic cations at B site was synthesized in the 1960s.[10] Its unique perovskite structure (Fig. 1) was later determined by x-ray diffraction.[11] The magnetic ground state of $CaCu_3Ti_4O_{12}$ was found to be antiferromagnetic with the Néel temperature of $T_N = 25$ K.[12,13] It has also been extensively studied owing to its enormous dielectric response.[14,15] By contrast, $CaCu_3Ge_4O_{12}$ and $CaCu_3Sn_4O_{12}$ were found to be ferromagnetic with the Curie temperature of $T_C = 13$ K and $T_C = 10$ K, respectively.[16,17] Although it has not been synthesized yet, predictive calculations of $CaCu_3Zr_4O_{12}$ are also included in this study so as to compare the magnetic properties in the series. Recently, Mizumaki *et al.* have performed oxygen K-edge x-ray absorption spectroscopy (XAS) measurement in $CaCu_3B_4O_{12}$ (B = Ti, Ge, and Sn) in order to discuss the orbital hybridization and the magnetic coupling.[18] They have concluded as follows: (i) ferromagnetism in $CaCu_3Ge_4O_{12}$ and $CaCu_3Sn_4O_{12}$ is stabilized by direct-exchange interaction between neighboring Cu^{2+} spins [corresponding to J_1 in Fig. 1(b)], (ii) Cu-O-Cu path (J_2) plays a less important role in magnetic interaction, and (iii) antiferromagnetism in $CaCu_3Ti_4O_{12}$ is stabilized by long-range superexchange interaction through the Cu-O-Ti-O-Cu interaction path (J_3). The importance of J_3 has also been pointed out in a theoretical study by Lacroix.[19]

In this paper, we investigate magnetic properties of $CaCu_3B_4O_{12}$ by *ab initio* calculations in order to quantitatively confirm the magnetic interaction of Cu^{2+} spins. There have been several *ab initio* studies on $CaCu_3Ti_4O_{12}$ in literature,[15,20–23] but most of them are focusing on its dielectric properties. The magnetic exchange interaction in $CaCu_3Ti_4O_{12}$ has been investigated by Johanness and Pickett[24] with a tight-binding model. The magnetism in $CaCu_3B_4O_{12}$ oxides has been discussed in a series of calculations by Xiang and coworkers.[25–29] However, the magnetic exchange interaction has not been evaluated and the detailed mechanism for the magnetic coupling is still unclear. In the following, first we show the computational results on the magnetic interaction, and then carefully discuss the physical mechanism behind them.

II. METHODOLOGY

DFT calculations were performed using the VASP code[32–35] and the PAW pseudopotentials[36,37] within the GGA-PBE formalism[38,39] in order to extract the electronic and magnetic properties. Wave functions of the valence electrons are expanded on a plane wave basis up to a cutoff energy of 500 eV. For most of the calculations, a $6 \times 6 \times 6$ Monkhorst-Pack k-point grid[40] was used for the Brillouin zone integration. Both the internal atomic coordinates and the lattice vectors of the crystal structure are optimized starting from the experimental data.[30,31] A threshold on the atomic forces for optimization is set as 1 meV/Å.

Maximally localized Wannier functions (MLWFs) were calculated by using WANNIER90 package.[41,42] The interface

 ©2013 American Physical Society

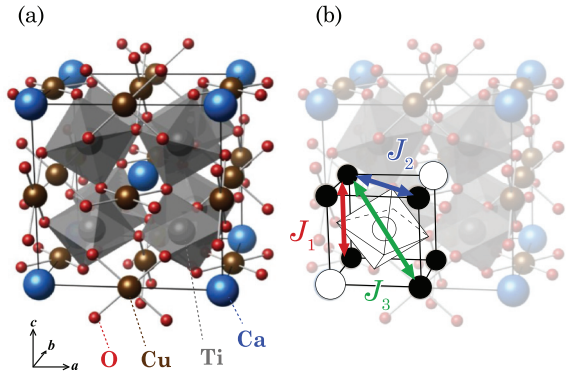

FIG. 1. (Color online) (a) Crystal structure of $CaCu_3Ti_4O_{12}$. (b) Exchange interaction between spin at Cu sites, J_1, J_2, and J_3 (see text).

was recently incorporated in the VASP code. A MLWF $|w_{n\boldsymbol{R}}\rangle$ specified by band index n and lattice vector $\boldsymbol{R}$ is defined as a Fourier transform of Bloch functions $|\psi_{m\boldsymbol{k}}\rangle$ with unitary transformation,

$$|w_{n\boldsymbol{R}}\rangle = \frac{V}{(2\pi)^3}\int_{\mathrm{BZ}}\left[\sum_{m=1}^{N} U_{mn}^{(\boldsymbol{k})}|\psi_{m\boldsymbol{k}}\rangle\right] e^{-i\boldsymbol{k}\cdot\boldsymbol{R}} d\boldsymbol{k}, \qquad (1)$$

where $\boldsymbol{k}$ is the wave vector of Bloch functions and $U_{mn}^{(\boldsymbol{k})}$ is the unitary transformation matrix that mixes the bands at wave vector $\boldsymbol{k}$. A unique choice of $U_{mn}^{(\boldsymbol{k})}$ is determined by minimizing the total quadratic spread of the Wannier functions. In our calculations, the initial projection of the Bloch bands of occupied Cu-d states was taken onto five cubic-harmonic $3d$ orbitals, namely $d_{3z^2-r^2}$, $d_{x^2-y^2}$, d_{xy}, d_{yz}, and d_{xz}. A set of MLWFs in the majority spin channel for each Cu site were obtained by iterative minimization of the quadratic spread. Once $U_{mn}^{(\boldsymbol{k})}$ was determined, transfer integrals between the MLWFs were calculated as the Hamiltonian matrix element,

$$t_{nm} \equiv \langle w_{n\boldsymbol{0}}|\hat{H}|w_{m\boldsymbol{0}}\rangle = \frac{V}{(2\pi)^3}\int_{\mathrm{BZ}}\left[\sum_{l}\left(U_{ln}^{(\boldsymbol{k})}\right)^{*}\epsilon_{l\boldsymbol{k}}U_{lm}^{(\boldsymbol{k})}\right] d\boldsymbol{k}, \qquad (2)$$

where $\epsilon_{l\boldsymbol{k}}$ is the eigenvalue corresponding to $|\psi_{l\boldsymbol{k}}\rangle$. In the calculation of transfer integrals, a $10\times10\times10$ uniform grid was used for the k-point sampling to achieve enough convergence.

III. RESULT AND DISCUSSION

A. Magnetic stability and exchange interaction

The optimized structural parameters (such as Cu-O bond length and Cu-O-Cu bond angle) show good agreement with the experiment, as tabulated in Table I. The lattice constant a is systematically overestimated by about 1%, as commonly seen when a GGA functional is used for the exchange-correlation energy.

The magnetic stability was derived from comparison of total energy which was calculated by imposing ferromagnetic (FM) and G-type antiferromagnetic (AFM-1) spin configurations (see Fig. 2), where the optimization of crystal structure was separately performed for each spin configuration. Note that a system with AFM-1 spin order has $Pm\bar{3}$ symmetry that is lower than the original symmetry of the crystal ($Im\bar{3}$). For the sake of accurate comparison of total energies, the calculations were done always with $Pm\bar{3}$ symmetry even for the FM phase. The trend of the magnetic stability ΔE (shown in Table I) is in reasonable agreement with the experiment.

TABLE I. Calculated structural parameters at the optimized crystal structure (lattice constant a, Cu-O bond length $d_{\text{Cu-O}}$, and Cu-O-Cu bond angle $\phi_{\text{Cu-O-Cu}}$), total energy difference between FM and AFM spin configurations $\Delta E = E_{\text{FM}} - E_{\text{AFM}}$, and local moments on Cu and O atoms (m_{Cu} and m_{O}), along with the magnetic transition temperatures estimated within the mean-field approximation (see text). The corresponding experimental data are also shown for comparison.[30,31]

B element	Ge	Ti	Sn	Zr
Calculation				
a (Å)	7.353	7.470	7.773	7.861
$d_{\text{Cu-O}}$ (Å)	1.985	1.978	1.999	2.002
$\phi_{\text{Cu-O-Cu}}$ (deg)	100.40	100.55	100.97	100.84
ΔE (meV/f.u.)	−7.82	54.00	−4.72	33.90
m_{Cu} (μ_{B})	0.580	0.501	0.567	0.538
m_{O} (μ_{B})	0.090	0.070	0.091	0.079
$T_{\text{C,N}}$ (K)	30.5	69.8	26.0	50.7
Experiment				
$r_{\text{ion}}(B)$ (Å)	0.53	0.605	0.69	0.72
a (Å)	7.267	7.391	7.642	
$d_{\text{Cu-O}}$ (Å)	1.982	1.971	1.987	
$\phi_{\text{Cu-O-Cu}}$ (deg)	100.67	100.76	100.68	
Magnetism	FM	AFM	FM	
$T_{\text{C,N}}$ (K)	13	25	10	

The calculated density of states (DOS) are summarized in Fig. 3. The overall feature is similar among the oxides, except that the B-d^0 state is found at a few eV above the valence band maximum (VBM) for B = Ti and Zr but not for B = Ge and Sn. The valence band states mainly consist of hybridized O-p and Cu-d states. All the oxides are calculated as insulators with band gap energy $E_g \approx 0.5$–1.0 eV, even though we used a GGA exchange-correlation functional that is known to underestimate E_g. The Cu-d state exhibits crystal field splitting due to the ligand O^{2-} ions in the square planar coordination (note that the point symmetry of Cu-12a site is $mm2$ that lacks the fourfold rotation and does not cause

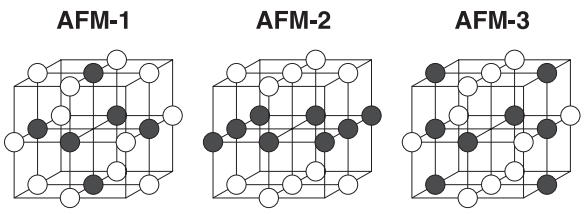

FIG. 2. Magnetic configurations of the A'-site sublattice. The up- and down-spin sites are represented by the open and filled circles, respectively.

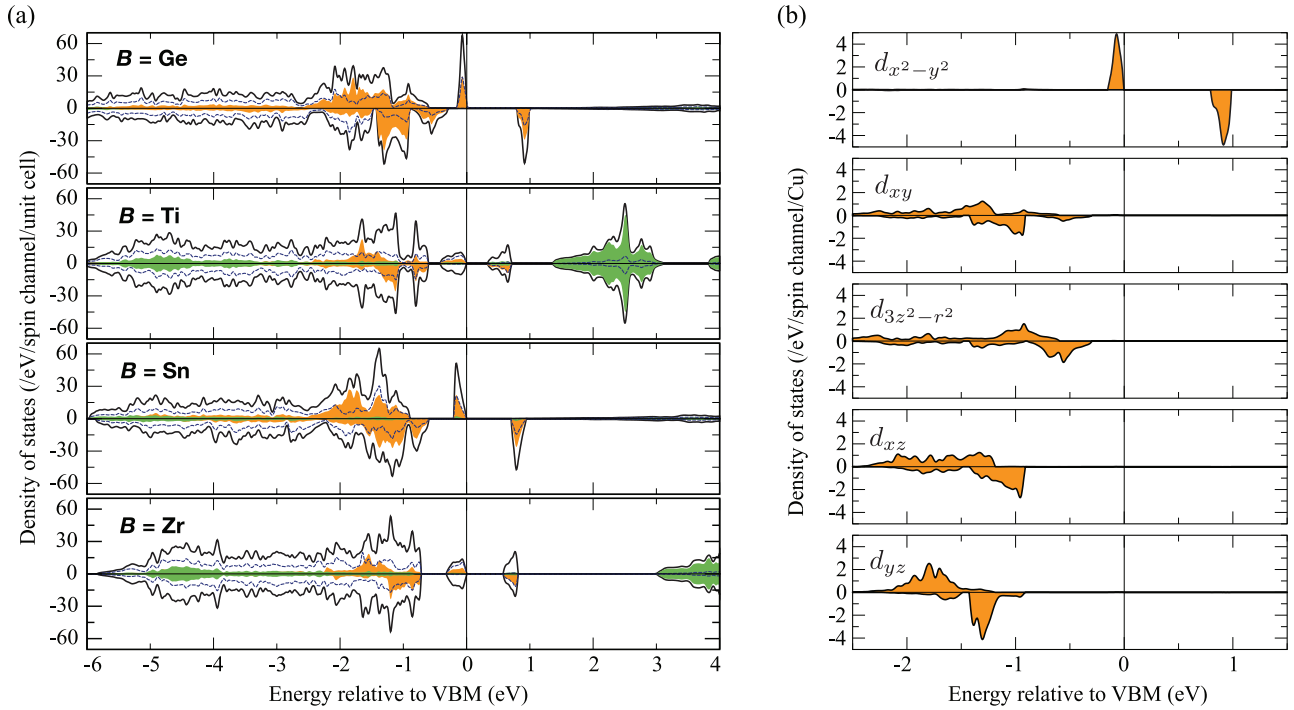

FIG. 3. (Color online) (a) Density of states (DOS) of $CaCu_3Ge_4O_{12}$, $CaCu_3Ti_4O_{12}$, $CaCu_3Sn_4O_{12}$, and $CaCu_3Zr_4O_{12}$. Total DOS is shown by the solid line. Partial DOS of Cu, *B*, and O atoms are shown by the orange shaded area, the green shaded area, and the blue dotted line, respectively. (b) Orbital-decomposed partial DOS of Cu *d* state in $CaCu_3Ge_4O_{12}$.

degeneration of d_{xz} and d_{yz} orbitals). By looking at the orbital-decomposed DOS, highest occupied and lowest unoccupied orbital states are found to be $d_{x^2-y^2}$ states that have lobes pointing toward the nearest ligand O^{2-} ions.

The magnetic exchange coupling constants J_{ij} were estimated by using the calculated magnetic energy fitted to an effective classical Heisenberg Hamiltonian,[43]

$$H = -\frac{1}{2}\sum_{i\neq j} J_{ij}\boldsymbol{e}_i \cdot \boldsymbol{e}_j, \tag{3}$$

where $\boldsymbol{e}_i$ is the direction of localized magnetic moment at site i and the factor of $1/2$ is multiplied to cancel double counting. We focus on the exchange parameters between the first-, second-, and third-nearest-neighbor Cu^{2+} ions, i.e., J_1, J_2, and J_3, respectively (see Fig. 1). In order to derive these parameters, four different types of collinear magnetic configurations are considered: ferromagnetic (FM), *G*-type antiferromagnetic (AFM-1), layered *A*-type-like antiferromagnetic (AFM-2), and another type of antiferromagnetic (AFM-3) configuration as depicted in Fig. 2. Equation (3) is then reduced to

$$\begin{aligned} E_{\mathrm{FM}} &= -12J_1 - 24J_2 - 24J_3, \\ E_{\mathrm{AFM\text{-}1}} &= 12J_1 - 24J_2 + 24J_3, \\ E_{\mathrm{AFM\text{-}2}} &= -4J_1 + 8J_2 + 24J_3, \\ E_{\mathrm{AFM\text{-}3}} &= 4J_1 + 8J_2 - 8J_3. \end{aligned} \tag{4}$$

The ferromagnetic and antiferromagnetic transition temperatures (T_{C} and T_{N}) are calculated within the mean-field approximation[43] as follows:

$$T_{\mathrm{C}} = \frac{2}{3k_{\mathrm{B}}}(2J_1 + 4J_2 + 4J_3), \tag{5}$$

$$T_{\mathrm{N}} = \frac{2}{3k_{\mathrm{B}}}(-2J_1 + 4J_2 - 4J_3), \tag{6}$$

where k_{B} is the Boltzmann constant.

Calculated values of J_{ij} are shown in Fig. 4. In this calculation, both the size and direction of Cu^{2+} spin moments were constrained via a penalty energy function so as to forcefully realize unstable AFM-2 and AFM-3 configurations in which otherwise the moments would be decreased. The Curie and Néel temperatures evaluated from J_{ij} are listed in Table I. Although the calculated values are 2–3 times higher than the experimental values, the chemical trends of the transition temperatures qualitatively agree with the

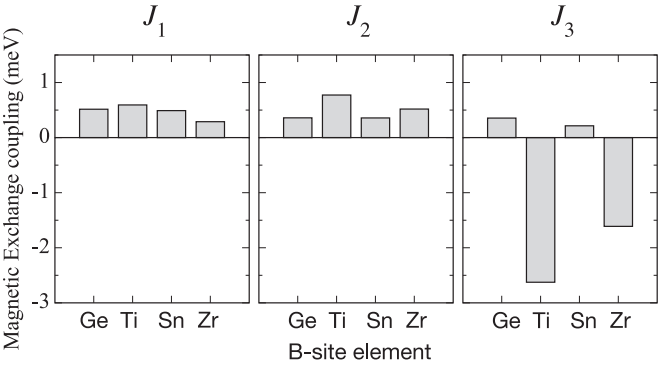

FIG. 4. Estimated magnetic exchange coupling constants.

experiment. Considering that the mean-field approximation generally overestimates transition temperatures, the values of T_C, T_N, and hence J_{ij} seem to be estimated successfully within the present framework.

As shown in Fig. 4, the dependence on replacement of the B-site element is clearly seen in J_3, whereas it is much more subtle in J_1 and J_2. The strong B-site-element dependence of J_3 implies a large contribution from long-range superexchange interaction through the Cu-O-B-O-Cu paths, as suggested by Lacroix.[19] On the other hand, the weak B-site-element dependence of J_1 and J_2 can be regarded as either Cu-Cu direct exchange as suggested by Shiraki *et al.*,[17] or Cu-O-Cu superexchange interaction.

Although we only consider J_1, J_2, and J_3 in this paper, it should be noted that there is possibly a contribution of interactions beyond J_3. For example, Johannes and Pickett have pointed out that even J_5 has non-negligible contribution to the magnetic order of $CaCu_3Ti_4O_{12}$.[24] However, since they also showed that the dominant interaction is J_3, we believe that exchange interactions up to the third neighbors are enough to explain the fundamental mechanism for the magnetic ordering.[44] The calculations of the further long-range interactions, in which supercells would be required, are left for future works. In the following subsections, we will carefully discuss the microscopic mechanism behind J_1, J_2, and J_3.

B. Wannier representation of d-d interaction

In order to elucidate the mechanism behind J_1, the MLWFs of Cu-d orbitals and the transfer integrals were calculated. A selected set of the MLWFs in $CaCu_3Ti_4O_{12}$ are shown in Fig. 5. A pair of neighboring Cu^{2+} ions, named Cu1 and Cu2 hereinafter, are considered. Note that they have different ligand planes perpendicular to each other as shown in Fig. 5(a), and that, therefore, the orbitals are labeled differently based on each

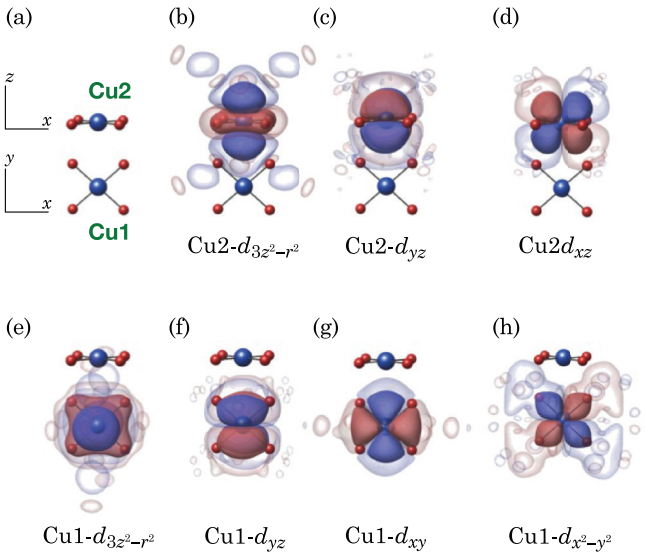

FIG. 5. (Color online) Maximally localized Wannier functions of Cu-d states in $CaCu_3Ti_4O_{12}$. Two isosurfaces are plotted: one at a high isovalue with dark color to show its original atomiclike nature, and the other at a low isovalue with transparent color to show its spatial distribution.

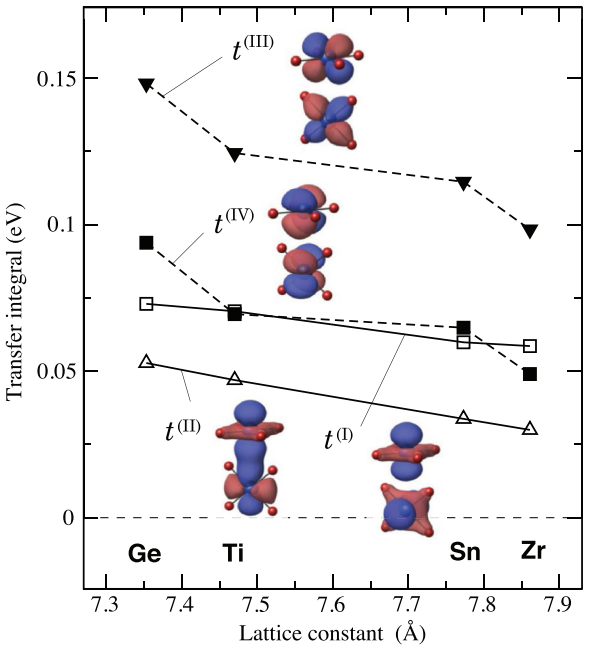

FIG. 6. (Color online) Transfer integrals between intersite MLWFs as a function of the lattice constant. The shapes and orientations of MLWFs are also schematically shown. The $dd\sigma$ hopping integrals ($t^{(I)}$ and $t^{(II)}$) are plotted with open symbols, and the $dd\pi$ hopping integrals ($t^{(III)}$ and $t^{(IV)}$) with closed symbols.

local frame. Among all the 25 orbital pairs, transfer integrals are found to be large in the following pairs of orbitals: $t^{(I)} = {}_1\langle 3z^2 - r^2|\hat{H}|3z^2 - r^2\rangle_2$, $t^{(II)} = {}_1\langle xy|\hat{H}|3z^2 - r^2\rangle_2$, $t^{(III)} = {}_1\langle x^2 - y^2|\hat{H}|xz\rangle_2$, and $t^{(IV)} = {}_1\langle yz|\hat{H}|yz\rangle_2$, where the bra and ket states denote the orbitals at Cu1 and Cu2, respectively. According to the spatial orientation of each orbital (the schematic illustration is given in Fig. 6), we classify the pairs into $dd\sigma$ ($t^{(I)}$ and $t^{(II)}$) and $dd\pi$ ($t^{(III)}$ and $t^{(IV)}$). The values are shown in Fig. 6, revealing that $t^{(III)}$ has the largest value. This is somewhat unexpected because $dd\sigma$ hopping is generally greater than $dd\pi$ hopping for atomic orbitals, but not surprising if considering the fact that the lobes of $|x^2 - y^2\rangle$ orbital are elongated due to the hybridization with O-p state as seen in Fig. 5(h). The strong $d_{x^2-y^2}$-p hybridization would be one of the characteristics of the family of the compounds, which is given rise to by the peculiar crystal structure. Since it is found that the d-d transfer is assisted by O-p orbitals, the mechanism behind J_1 might be understood by superexchange interaction rather than direct exchange interaction.

C. Superexchange interaction

To simulate the superexchange interaction paths of J_1 and J_2, a simple model with atomic orbitals is considered. As shown in Fig. 7, there are three Cu^{2+} ions (Cu1, Cu2, and Cu3) and an O^{2-} ion lying on a same plane. The paths along Cu1-O-Cu2 and Cu1-O-Cu3 correspond to J_1 and J_2, respectively. In order to simplify the following discussion, we assume that the O^{2-} ion is located at the equidistant position from all the Cu^{2+} ions and thus the bond angle for J_1 is 90°. Since both the highest occupied and lowest unoccupied states are $d_{x^2-y^2}$ orbital states, which are well separated from the

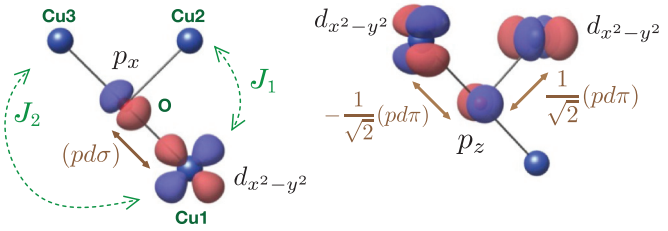

FIG. 7. (Color online) Schematic configuration of atomic orbitals and the two-center transfer integrals between Cu-$d_{x^2-y^2}$ and O-p orbitals.

other d orbitals, it would be possible to assume that $d_{x^2-y^2}$ orbital dominantly contributes to superexchange interaction. Let us denote each $d_{x^2-y^2}$ orbital on Cu^{2+} ions as d_1, d_2, and d_3, and the transfer integrals between d_i and one of the O-p orbitals as t_i. If electrons can virtually transfer from d_i to d_j through a single O-p orbital, the superexchange interaction is antiferromagnetic[45] and the energy gain is derived by fourth-order perturbation[46] as

$$E^{(4)} \approx -\frac{2|t_i t_j|^2}{\Delta^2}\left(\frac{1}{\Delta}+\frac{1}{U_{\rm eff}}\right), \tag{7}$$

where Δ is the p-d charge transfer energy and $U_{\rm eff}$ the effective on-site Coulomb energy of d electrons. If electrons transfer through two different O-p orbitals, the superexchange becomes ferromagnetic[45] with the energy gain

$$E^{(4)} \approx -\frac{4|t_i t_j|^2}{\Delta^2}\left(\frac{1}{2\Delta}-\frac{1}{2\Delta-J_H}\right) \approx \frac{|t_i t_j|^2}{\Delta^4}J_H, \tag{8}$$

where J_H is the Hunt's coupling energy in O-p orbitals and the last expression is obtained by assuming that $\Delta \gg J_H$.

By means of the two-center Slater-Koster (SK) parameters,[47] the transfer integrals t_i are estimated as follows: $t_1 = (pd\sigma)$, $t_2 = \frac{1}{\sqrt{2}}(pd\pi)$, and $t_3 = -\frac{1}{\sqrt{2}}(pd\pi)$. The corresponding orbital combinations are shown in Fig. 7, and all the other combinations lead to exactly zero transfer integral due to the symmetry of the orbitals. Since possible superexchange paths are d_1-p_x:p_z-d_2 for J_1 and d_1-p_x:p_z-d_3 for J_2, both of them are expected to be ferromagnetic. Furthermore, interestingly, as the magnitude of t_2 and t_3 are equivalent, the energy gain (8) should also be comparable between J_1 and J_2. This makes a clear contrast to conventional perovskite oxides, where the superexchange interaction changes the sign and strength when the bond angle changes from 90° to 180°.[8,9,48] In the A-site-ordered perovskite structure, the ligand planes around neighboring A' sites are perpendicular to each other, so that the effect of 90° rotation in the bond angle is canceled by the corresponding 90° rotation of the ligand planes. This model might be too simplistic but seems to reasonably explain our numerical results for J_1 and J_2.

D. Long-range superexchange interaction

In order to analyze J_3 interaction, the partial charge and magnetization density is calculated within an energy window from $E_{\rm min} = E_{\rm VBM}$ to $E_{\rm max} = E_{\rm VBM} + 1$ eV. This energy range corresponds to the upper Hubbard band (UHB) that consists mainly of the hybridized Cu-$d_{x^2-y^2}$ and O-p state.

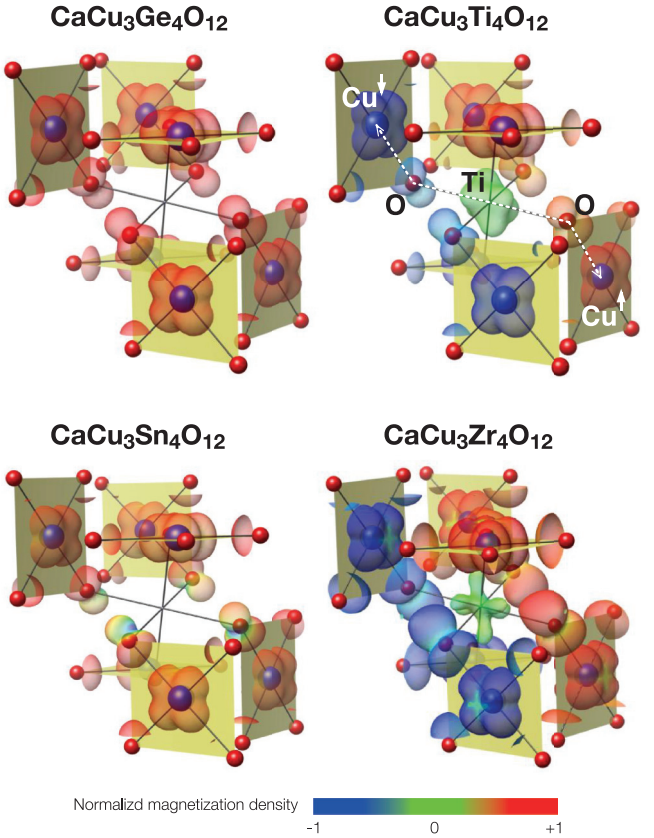

FIG. 8. (Color online) Partial charge density of $CaCu_3Ge_4O_{12}$ (top left), $CaCu_3Ti_4O_{12}$ (top right), $CaCu_3Sn_4O_{12}$ (bottom left), and $CaCu_3Zr_4O_{12}$ (bottom right) for the upper Hubbard band. The magnetization density is shown by the surface coloring. The B atoms are located at each center but not shown for the sake of visibility. An arbitrarily chosen isovalue is used for the former three compounds, while a smaller isovalue is used for the latter in order to magnify the charge.

Figure 8 shows the partial charge density around a B atom and its neighboring six CuO_4 planes. The surface coloring of the charge density cloud indicates its spin polarization: the red and blue regions present spin polarization in one spin channel opposite to each other, while the green region shows that the charge has no spin polarization. The cloud of the UHB (that consists mainly of Cu-$d_{x^2-y^2}$ and O-p_x states) and its spin order are clearly seen in Fig. 8. In the antiferromagnetic oxides (B = Ti and Zr), a cloud of charge density is also found around Ti and Zr atom. This shows that the UHB has hybridization with the empty Ti-d and Zr-d states that lie a few eV above the UHB. On the other hand, no state is found around Ge and Sn atom, showing that the Ge-d and Sn-d states have no hybridization with the UHB because they are fully occupied and located well below the Fermi level. Orbital expansion of the state around Ti and Zr atoms in cubic harmonics (with axes parallel to the B-O bonds) reveals that it consists mainly of the B-t_{2g} state with lobes pointing to the space between the B-O bonds. Each B-t_{2g} state has π-type overlap with two neighboring O-p_x states in the opposite direction to each other. When spins on the O-p states are antiparallel, both of them can transfer to the empty B-t_{2g} state at the same time, while it is prohibited for parallel spins by Pauli's exclusion principle.

Therefore, the antiparallel spin configuration leads to energy gain by making an interaction path along Cu-O-*B*-O-Cu as shown by the dotted line in Fig. 8.

As we saw in Fig. 4, this interaction is stronger than J_1. This is because it can be regarded as a typical 180° antiferromagnetic superexchange interaction (if we assume the hybridized Cu-$d_{x^2-y^2}$ and O-p_x states as a single orbital), while the ferromagnetic J_1 interaction is basically similar to a typical 90° superexchange interaction that is generally weak. Therefore, our conclusion is that, in the family of the oxides considered in this paper, the spin order depends mostly on the fact whether antiferromagnetic J_3 interaction works or not, and that the key factor here is the presence of the empty t_{2g} d states of the B atoms.

IV. SUMMARY

Magnetic exchange interaction in A-site-ordered perovskites $CaCu_3Ge_4O_{12}$, $CaCu_3Ti_4O_{12}$, $CaCu_3Sn_4O_{12}$, and $CaCu_3Zr_4O_{12}$ has been investigated. The magnetic ordering in the ground state is found to be realized by the nearest-neighbor ferromagnetic interaction J_1 in $CaCu_3Ge_4O_{12}$ and $CaCu_3Sn_4O_{12}$, but by the third-nearest-neighbor antiferromagnetic interaction J_3 that overwhelms J_1 in $CaCu_3Ti_4O_{12}$ and $CaCu_3Zr_4O_{12}$. The underlying mechanism of J_1 is speculated as the Cu-O-Cu superexchange interaction that is almost independent to the B-site element and is explained to be weakly ferromagnetic by a simplified cluster model with atomic orbitals. The cluster model reveals that the same mechanism is also applied for the second-nearest-neighbor interaction J_2. In contrast, the mechanism of J_3 is considered to be the long-range superexchange interaction along Cu-O-*B*-O-Cu path that works selectively when the B-t_{2g} state is available. The strong hybridization between Cu-$d_{x^2-y^2}$ and O-p orbitals seems to be one of the characteristic features of this family as it reflects the crystal structure and contributes all of J_1, J_2, and J_3.

ACKNOWLEDGMENTS

We thank Dr. Y. Shimakawa and Dr. M. Mizumaki for helpful correspondence. We also acknowledge suggestions on analysis of superexchange interaction given by Dr. P. Barone. The computation in this work has been partly done using the facilities of the Supercomputer Center, the Institute for Solid State Physics, the University of Tokyo. This work was supported by the CREST program of the Japan Science and Technology Agency.

*toyoda-cmp@sanken.osaka-u.ac.jp

[1] J. Bednorz and K. Müller, Z. Phys. B **64**, 189 (1986).
[2] G. Jonker and J. Van Santen, Physica **16**, 337 (1950).
[3] J. Van Santen and G. Jonker, Physica **16**, 599 (1950).
[4] A. Bussmann-Holder, J. Phys.: Condens. Matter **24**, 273202 (2012).
[5] W. Prellier, M. Singh, and P. Murugavel, J. Phys.: Condens. Matter **17**, R803 (2005).
[6] D. Serrate, J. De Teresa, and M. Ibarra, J. Phys.: Condens. Matter **19**, 023201 (2007).
[7] P. Alippi and V. Fiorentini, Eur. Phys. J. B **85**, 82 (2012).
[8] J. B. Goodenough, Phys. Rev. **100**, 564 (1955).
[9] J. Kanamori, J. Phys. Chem. Solids **10**, 87 (1959).
[10] A. Deschanvres, B. Raveau, and F. Tollermer, Bull. Soc. Chim. Fr. **11**, 4077 (1967).
[11] B. Bochu, M. N. Deschizeaux, J. C. Joubert, A. Collomb, J. Chenavas, and M. Marezio, J. Solid Sate Chem. **29**, 291 (1979).
[12] A. Collomb, D. Samaras, B. Bochu, and J. C. Joubert, Phys. Status Solidi A **41**, 459 (1977).
[13] A. Koitzsch, G. Blumberg, A. Gozar, B. Dennis, A. P. Ramirez, S. Trebst, and S. Wakimoto, Phys. Rev. B **65**, 052406 (2002).
[14] M. Subramanian, D. Li, N. Duan, B. Reisner, and A. W. Sleight, J. Solid State Chem. **151**, 323 (2000).
[15] L. He, J. B. Neaton, M. H. Cohen, D. Vanderbilt, and C. C. Homes, Phys. Rev. B **65**, 214112 (2002).
[16] Y. Ozaki, M. Ghedira, J. Chenavas, J. C. Joubert, and M. Marezio, Acta Crystallogr. Sect. B **33**, 3615 (1977).
[17] H. Shiraki, T. Saito, T. Yamada, M. Tsujimoto, M. Azuma, H. Kurata, S. Isoda, M. Takano, and Y. Shimakawa, Phys. Rev. B **76**, 140403(R) (2007).
[18] M. Mizumaki, T. Saito, H. Shiraki, and Y. Shimakawa, Inorg. Chem. **48**, 3499 (2009).
[19] C. Lacroix, J. Phys. C: Solid State Phys. **13**, 5125 (1980).
[20] L. He, J. B. Neaton, D. Vanderbilt, and M. H. Cohen, Phys. Rev. B **67**, 012103 (2003).
[21] S. Matar and M. Subramanian, Mater. Lett. **58**, 746 (2004).
[22] S. B. Fagan, A. G. Souza Filho, A. P. Ayala, and J. Mendes Filho, Phys. Rev. B **72**, 014106 (2005).
[23] C. McGuinness, J. E. Downes, P. Sheridan, P.-A. Glans, K. E. Smith, W. Si, and P. D. Johnson, Phys. Rev. B **71**, 195111 (2005).
[24] M. Johannes and W. Pickett, Acta Phys. Pol. B **34**, 1553 (2003).
[25] H. Xiang, X. Liu, E. Zhao, J. Meng, and Z. Wu, Appl. Phys. Lett. **91**, 011903 (2007).
[26] H. Xiang, X. Liu, E. Zhao, J. Meng, and Z. Wu, Inorg. Chem. **46**, 9575 (2007).
[27] H. Xiang and Z. Wu, Inorg. Chem. **47**, 2706 (2008).
[28] H. Xiang, X. Liu, J. Meng, and Z. Wu, J. Phys.: Condens. Matter **21**, 045501 (2009).
[29] S. Lv, X. Liu, H. Li, D. Han, and J. Meng, J. Phys. Chem. C **115**, 2366 (2011).
[30] R. Shannon, Acta Crystallogr. Sect. A **32**, 751 (1976).
[31] Y. Shimakawa, Inorg. Chem. **47**, 8562 (2008).
[32] G. Kresse and J. Hafner, Phys. Rev. B **47**, R558 (1993).
[33] G. Kresse and J. Hafner, Phys. Rev. B **49**, 14251 (1994).
[34] G. Kresse and J. Furthmüller, Phys. Rev. B **54**, 11169 (1996).
[35] G. Kresse and J. Furthmüller, Comput. Mater. Sci. **6**, 15 (1996).
[36] P. E. Blöchl, Phys. Rev. B **50**, 17953 (1994).
[37] G. Kresse and D. Joubert, Phys. Rev. B **59**, 1758 (1999).
[38] J. P. Perdew, K. Burke, and M. Ernzerhof, Phys. Rev. Lett. **77**, 3865 (1996).
[39] J. P. Perdew, M. Ernzerhof, and K. Burke, Phys. Rev. Lett. **78**, 1396 (1997).
[40] H. J. Monkhorst and J. D. Pack, Phys. Rev. B **13**, 5188 (1976).

[41]N. Marzari and D. Vanderbilt, Phys. Rev. B **56**, 12847 (1997).
[42]I. Souza, N. Marzari, and D. Vanderbilt, Phys. Rev. B **65**, 035109 (2001).
[43]A. Liechtensiten, M. Katsnelson, V. Antropov, and V. Gubanov, J. Magn. Magn. Mater. **67**, 65 (1987).
[44]From the MLWFs calculated in Sec. III B, t_5 is estimated to be 2–3 orders of magnitude smaller than t_3. Therefore, as regards the direct exchange interaction ($J = 4t^2/U$), J_5 in our calculations is about five orders of magnitude smaller than J_3.
[45]K. Yosida, *Theory of Magnetism* (Springer-Verlag, New York, 1998).
[46]Here, we assume $|t| \ll |\Delta|$ for perturbation expansion. However, the validity of the assumption is not so obvious for copper oxides, where $|\Delta|$ can be very small. Although those tight-binding parameters were not numerically estimated, we can make a rough estimation from the density of states (Fig. 3). $|\Delta|$ corresponds to the energy difference between the top of O-p band and the unoccupied $d_{x^2\text{-}y^2}$ state, which is $\simeq$1–2 eV. $|t|$ is known to scale with the bandwidth of $d_{x^2\text{-}y^2}$, that is $\simeq$0.2–0.3 eV. Therefore, we expect that the assumption still holds.
[47]J. C. Slater and G. F. Koster, Phys. Rev. **94**, 1498 (1954).
[48]P. W. Anderson, Phys. Rev. **79**, 350 (1950).